Widely Tunable Monolithically Integrated All-Optical Wavelength Converters in InP

Milan L. Mašanović, *Member, IEEE*, Vikrant Lal, *Student Member, IEEE*, Joseph A. Summers, *Student Member, IEEE*, Jonathon S. Barton, *Student Member, IEEE*, Erik J. Skogen, Lavanya G. Rau, Larry A. Coldren, *Fellow, IEEE, Fellow, OSA*, and Daniel J. Blumenthal, *Fellow, IEEE, Member, OSA*

***Abstract*—Design, fabrication, and characterization of monolithically integrated widely tunable all-optical wavelength converters in InP is reported. The devices are based on the SGDBR laser integrated with different MZI-SOA wavelength converters. Error-free wavelength conversion at 2.5 Gbps was demonstrated over 50 nm input and 22 nm output wavelength range. Static operation, extinction ratio enhancement, signal reamplification, dynamic range, and chirp properties were characterized as well.**

***Index Terms*—Mach-Zehnder interferometer (MZI), photonic integrated circuits (PICs), tunable laser, tunable wavelength converter, wavelength conversion, wavelength converter.**

I. Introduction

THE further development of photonic integrated circuits (PICs) with increased functional complexity, monolithically integrated on a single chip, is a critical step for the future deployment of optical networks. Monolithically integrated widely tunable wavelength converters are a family of PICs whose function is essential for wavelength division multiplexing (WDM) systems, particularly in functions like optical switching, wavelength routing and add/drop multiplexing. The integration of tunable lasers and all-optical wavelength converters solves one of the last obstacles for all-optical switching to have the functionality and flexibility needed to be a serious candidate to replace electronic switches. Tunable all-optical wavelength converters allow data to be transferred from an input wavelength to a tunable output wavelength without passing the signal through electronics. Semiconductor optical amplifier Mach-Zehnder interferometer (SOA-MZI) wavelength converters represent an important class of integrated wavelength converters that work for both RZ and NRZ data formats while also acting as 2R signal regenerators due to their nonlinear transfer functions. Integration of SOA-MZIs in InP has been reported previously [1]–[3]. In addition, an SOA-MZI wavelength converter was integrated with a nontunable DFB laser, but it had severe performance tradeoffs due to reflections from the MZI back to the laser [4]. Recent attempts at an integrated multifrequency laser/MZI-SOA wavelength converter have shown an interesting device design concept, but have yet failed to produce a fully operational wavelength converter [5].

The devices reported in this paper consist of a widely tunable sampled grating distributed Bragg reflector (SGDBR) laser [6], monolithically integrated with different SOA-MZI wavelength converters [7], [8].

The SGDBR laser represents an enabling technology for widely tunable photonic integrated circuits. First, it is well suited for integration, as its lithographically defined mirrors enable lasing without a facet reflection [6]. Second, because the laser consists of a combination of active and passive waveguides, additional elements can be integrated on the same chip without increasing the level of complexity of the fabrication process. To illustrate the usefulness of SGDBR lasers, it is worth noting that in addition to our work described here, functional integration with other components has been reported for SOAs [9], EAMs [10], Mach-Zehnder modulators [11], and recently photocurrent-driven widely tunable wavelength converters [12], [13].

The fabrication platform used in this work, offset quantum wells, represents a versatile integration platform that enables simplicity in fabrication and high efficiency in transition between active and passive waveguides. Additionally, this platform, with its low contrast waveguides and the continuous quaternary waveguide layer throughout the entire device, is particularly suitable for reflection minimization and control, which is one of the key requirements for high-density PIC integration involving on-chip lasers. Using this platform, a single epitaxial overgrowth of p-InP is required to fabricate the devices, which makes the fabrication process simple, reproducible, and robust.

The level of chip-scale integration demonstrated in our tunable wavelength converters offers a number of benefits, some of which are: reduced coupling loss between the laser and the converter, reduced polarization control requirements, improved converter noise figure, higher conversion efficiency, and, ultimately, reduced size, simplified packaging, reduced footprint, and lower cost of the entire component.

II. Device Design and Fabrication

The integrated tunable wavelength converter consists of an InP SGDBR laser [6], monolithically integrated with an SOA-based MZI wavelength converter. The schematics of the two different device generations that have been designed, fabricated, tested, and are being described in this work are given in Figs. 2

Manuscript received November 14, 2003; revised August 28, 2004. This work was supported by DARPA/MTO CS-WDM Program by Grant N66001-02-C-8026.

M. L. Mašanović, V. Lal, J. A. Summers, J. S. Barton, L. A. Coldren, and D. J. Blumenthal are with the Electrical and Computer Engineering Department, University of California, Santa Barbara, CA 93106 USA (e-mail: mashan@ece.ucsb.edu).

E. J. Skogen is with the Sandia National Laboratories, Albuquerque, NM 87185 USA.

L. G. Rau is with the California Institute for Telecommunications and Information Technology, University of California, Irvine, CA 92697 USA.

Digital Object Identifier 10.1109/JLT.2005.843464

and 3. Both device generations use identical tunable laser designs and differ in the interferometric wavelength converter designs.

A. Tunable Laser Design

The SGDBR laser is 1.5 mm long and has five sections: front mirror, gain section, phase section, back mirror, and back facet detector. The back facet detector has been monolithically integrated for measurement of optical power and to decrease the requirements of the backside antireflective coating.

The laser's mirrors are made of periodically sampled DBR gratings that form a comb-like reflectivity spectrum which enables for wide tuning range using the Vernier effect [6]. The front mirror consists of five 4 μm long bursts spaced by 61.5 μm. The back mirror consists of twelve bursts that are 6 μm long and spaced by 46 μm. Since the sampling periods of the two mirrors differ, the peak reflectivity spacings are different, so that only one set of reflectivity peaks for both mirrors is aligned at one time. By differentially tuning the front or the back mirrors using electrical current injection, adjacent reflectivity peaks can be aligned, and the laser will operate at this new wavelength [6]. To achieve the wavelength coverage between the mirror peaks, both mirrors need to be tuned simultaneously.

B. MZI-SOA Design

The role of the MZI-SOAs is to behave as nonlinear elements and to enable the interaction between the continuous wave and the input data signals through the gain compression and phase change, which are used to achieve the wavelength converter operation. Two main MZI-SOA parameters of interest are the amount of phase change attainable, and the gain recovery lifetime, which will limit the maximum speed of operation. The dynamic response of an SOA depends on the material parameters of the SOA (differential gain), the level of electrical pumping, the confinement factor, the optical power in the SOA, as well as the length of the SOA through the effects of high-pass filtering [24]. While our material parameters (i.e., the gain as a function of carrier density) and the confinement factor (6%) are set by the choice of the integration platform, the other parameters can be adjusted, primarily by controlling the SOA's bias current, input optical power into the SOA and the length of the SOA.

Simulated total phase change in an SOA as a function of the optical power levels and the SOA lengths is shown in Fig. 1. The amount of the phase change will depend on the amount of index change, which in turn depends on the amount of the gain and carrier concentration change in the SOA. One disadvantage in using the offset quantum well platform is in the fact that the optical mode overlap with the active region is only 6%, and most of the index change happens in the active region (assuming large release times from the quantum wells). As a result, according to the simulation, large pump power variations are needed to achieve a full π rad phase shift. Analyzing Fig. 1, we conclude that increasing the length of the SOA beyond 1 mm will not significantly improve the phase change abilities. On the other hand, to utilize the full benefits of the self-filtering effect [24], the SOA length should be at least 1 mm. Extended SOA lengths will have an adverse effect in terms of possible back-reflections into the laser, heating, device power consumption and the chip

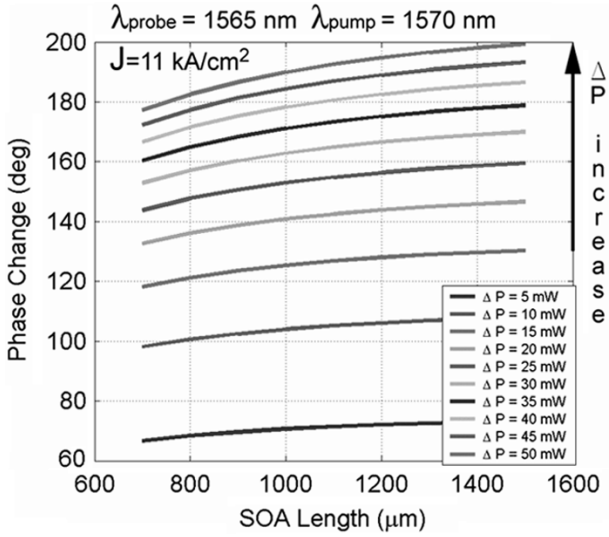

Fig. 1. Simulated phase change in a SOA as a function of the SOA length. The probe signal is kept constant at 4 mW and the power of the pump signal is varied.

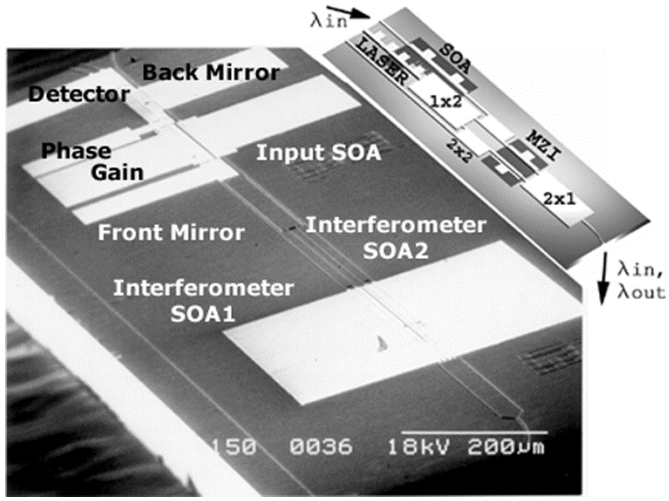

Fig. 2. Tunable all-optical MMI-MZI-based wavelength conveter (TAOMI-WC).

size. Taking all of these requirements and tradeoffs of our design into account, the optimum SOA length was chosen to be 1 mm.

C. Generation I—Tunable All-Optical MMI-MZI Wavelength Converter (TAOMI-WC)

In this device implementation, the interferometer is defined by a combination of two 16 μm wide and 760 μm long multimode interference (MMI) based 1×2 light splitters [15], in combination with 2 MMI based 2×2 couplers that are 12 μm wide [15], straight waveguides and 1 mm long SOAs (Fig. 2). The total waveguide separation in the interferometer is 17 μm. This value is determined primarily by the fabrication tolerances for the minimum separation of the two MZI-SOA electrodes. The input signal is coupled onto the chip through a tapered, angled input waveguide, and then amplified by an 800 μm long input semiconductor optical amplifier. The 2×2 MMI coupler is used to mix the input signal with the continuous wave signal generated by the SGDBR laser in one of the interferometer's

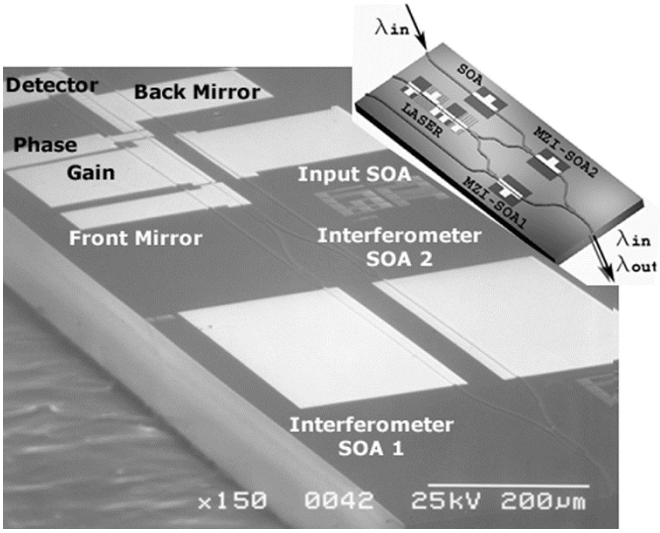

Fig. 3. Tunable all-optical MZI-based wavelength converter (TAO-WC).

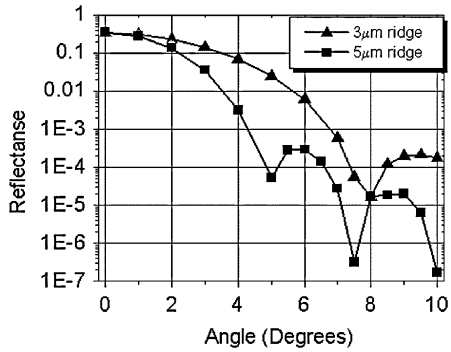

Fig. 4. Modal reflectance as function of the output waveguide width and angle.

SOAs. This SOA, where the interaction between the input data and the CW signal occurs, will be referred to as "common SOA" in the rest of this paper. The unused output branch of the 2×2 MMI coupler extends into the unpumped active region and is adiabatically tapered into a point to absorb all of the stray light. This is done to prevent any back reflections that could destabilize the laser. The output waveguide of the MZI is tapered and angled to reduce the AR coating requirements. The total device length is 5.2 mm.

D. Generation II—Tunable All-Optical MZI Wavelength Converter (TAO-WC)

The interferometer is defined by a combination of four 1×2 MMI light splitters and combiners (180 μm long and 13 μm wide), by S-bends with curvature radii of 2 mm and by two 1 mm long SOAs (Fig. 3). The laser and the interferometer are connected via a 1×2 MMI splitter and the total waveguide separation in the interferometer is 70 μm. This insures that there is no thermal crosstalk between the two branches of the interferometer. The input signal is coupled onto the chip through a tapered input waveguide, and then amplified by an 800 μm long input semiconductor optical amplifier. The same MMI splitter/combiner design is used to connect the input waveguide and the SGDBR signal with the common interferometer SOA, as well as to combine the light from the two branches at the interferometer output. The output waveguide is tapered and angled to reduce the AR coating requirements. The total device length is 4.9 mm.

E. Coherent Reflection Suppression

One of the critical design issues for PICs that include an integrated laser is the suppression of coherent back reflections. Low levels of coherent back-reflection will lead to an increase of the laser linewidth, while large back-reflections levels will be completely detrimental for device performance.

Several possible sources of reflection exist on our chips and they all require careful minimization. The potential sources of backreflection are the output facet, multimode interference based light splitters and combiners and the active-passive waveguide interfaces. The offset quantum-well integration platform, used in this paper, with its low refractive index contrast waveguides and the continuous quarternary waveguide layer throughout the entire device structure, is particularly suitable for reflection minimization and control.

The dominant source of back reflections is the output facet of the device. The SOAs of the Mach-Zehnder act as amplifiers for any reflections from the output facet. However, due to their operation in saturation, the amount of gain that they provide is limited to less than 8 dB. Taking into account the amplifier gain, to insure for linewidth change of less than 10%, the requirement for reflectance of the output facet is that it be better than 10^{-5}. This level of reflectance cannot be achieved by simple anti-reflection coating, rather, the output waveguide design has to minimize the amount of reflection. As has been proposed in [16], [17], angled output waveguides have significantly smaller modal reflectances than the corresponding straight waveguides. In addition, increasing the waveguide width further reduces the back reflection coupled into the original mode. Analiticaly, the reflectance of a Gaussian mode at an interface will have an exponential dependence on the angle of incidence and on the width of the mode [16]. Conversely, widening the output waveguide increases the ellipticity of the output mode, thereby complicating the coupling scheme required for high coupling efficiency. Fig. 4 shows the calculation of the modal reflectances [17] in function of the output waveguide angle, for two different output waveguide widths—3 μm and 5 μm. The values of the parameters in the calculation are based on the InP/InGaAsP material system used in this work. For the output angle of 6.5 degrees or higher, with the ridge with of 5 μm, the envelope of the modal reflectance will be lower than 10^{-4}. Therefore, applying a multilayer AR coating on this type of the output facet can provide for the broadband reflectance that meets our design requirements.

MMI-based components are a potential source of severe reflections, so care must be taken to optimize their design. This is especially true in integration platforms that utilize high index contrast waveguides [18]. Our fabrication platform, on the other hand, is based on the weakly guiding waveguides and employs no semiconductor-air interfaces. The MMI lengths in our structures are optimized for minimum back reflections according to [15], and all MMI components are tapered at both inputs and outputs so that reflections are not coupled back into the laser

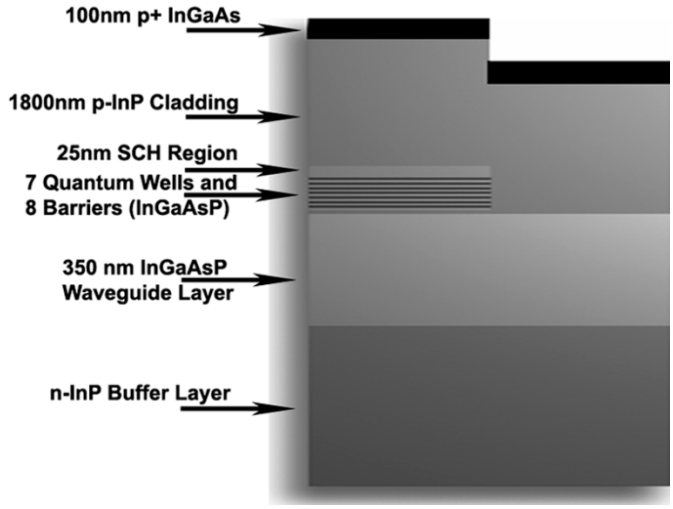

Fig. 5. Offset quantum well integration platform.

cavity. We found that this approach was easy to implement and as effective as the approach suggested in [19].

Low reflection, low loss transitions between the active and passive waveguides in our fabrication platform are achieved by employing techniques similar to those already discussed for the output waveguide design. Active-passive interfaces in the device are angled to avoid coupling of the reflected light into the waveguide mode. Moreover, the quarternary waveguide layer is continuous throughout the device structure, thereby avoiding potential index discontinuities such as those that can be introduced when using butt-joint growth techniques.

F. Fabrication

Devices are fabricated using an offset quantum well integration platform in InP. All growths are performed using the MOCVD crystal growth technology. The device cross section at the active-passive interface is shown in Fig. 5.

The layer formation of the base epitaxial structure consists of a 350 nm thick quarternary waveguide, followed by a 7 quantum well/8 barrier active region and a thin InP cap. The first step of the process is to selectively etch off the quantum wells in the future passive sections of the device. Subsequently, gratings are lithographically defined in the mirror sections using holography and then etched directly into the top of the waveguide layer using reactive ion etching (RIE). The surface of the sample is then regrown with a 1.8 μm thick p-doped InP upper cladding layer and a 100 nm p^+-InGaAs contact layer (Fig. 5). It is important to emphasize that this is the only regrowth step required in the entire process.

After the regrowth, ridges in InP are formed using a combination of RIE/crystallographic wet chemical etching. The surface of the sample is isolated with a dielectric film and the top metal contacts (Ti/Pt/Au—20/40/1000 nm) are evaporated using E-beam evaporation, followed by a proton implant to electrically isolate the different electrodes. After the sample is thinned down, identical back side (Ti/Pt/Au) contacts are evaporated and the sample is strip annealed at 420 °C. In conclusion, there are no additional major processing steps required to fabricate this device beyond the standard SGDBR fabrication process, which demonstrates the versatility of our integration platform.

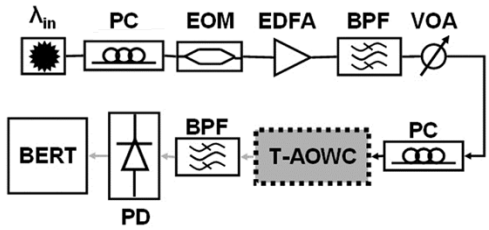

Fig. 6. Schematic of the test setup.

III. Experimental Procedure

All of the experiments are performed with the devices soldered on aluminum nitride submounts, wirebonded, vacuum clamped onto a gold-plated copper stage and cooled to 17 °C using a thermoelectric cooler. The light is coupled to and out of the devices using conical-tipped lensed-fibers mounted on the piezo-controlled translational stages. The tapered waveguides at device inputs and outputs improve the coupling to the device; we measured 4 dB of coupling loss to the waveguides on the chip. The input signal is generated using an external cavity tunable laser source and modulated using a lithium-niobate electrooptic modulator. Polarization controllers are used at both the input to the modulator and the wavelength converter because the device active regions are polarization sensitive. For static measurements, the output of the device is optically filtered and fed into an optical power meter. For wavelength conversion, the data is generated using a BERT with NRZ $2^{31}-1$ pseudorandom bit sequence (PRBS) data at 2.5 Gbps. The converted output wavelength is filtered using a 0.4-nm thin-film tunable filter and detected with a PIN receiver. The test setup schematic is shown in Fig. 6.

IV. Static Performance

The integrated tunable wavelength converter's lasers have a tuning range of about 22 nm—overlapped spectra for TAOMI-WC and TAO-WC devices are shown in Fig. 7(a) and (b). These spectra were recorded through the output facet of the device, with laser gain sections biased at 85 mA and both MZI SOAs biased at 200 mA. The tuning range is determined by the sampled mirror design, and could be extended to 40 nm by further optimization. The grating depth for TAOMI-WC devices is lower than for the TAO-WC devices, resulting in lower presence of the light reflected from the laser's rear mirror peaks in the overlapped spectra, shown in Fig. 7(b).

The output of the interferometer can be turned off by adjusting the bias of the SOA in one of the interferometer branches, in order to achieve π relative phase shift between the two branches. Fig. 8 shows an extinction map as a function of the currents applied to the SOAs in the interferometer arms. No input signal was present for these measurements. In the region of low bias currents ($<$120 mA), for one SOA current set, there exists a combination of currents where the extinction ratio is greater than or equal to 20 dB. However, with the increase in the SOA bias currents, the extinction ratio is reduced to as low as

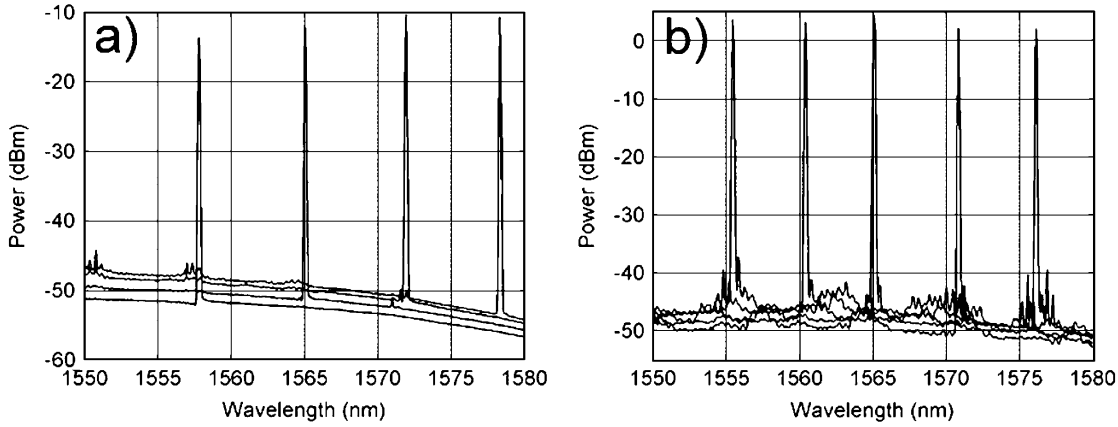

Fig. 7. Overlapped spectra for TAOMI-WC and TAO-WC devices.

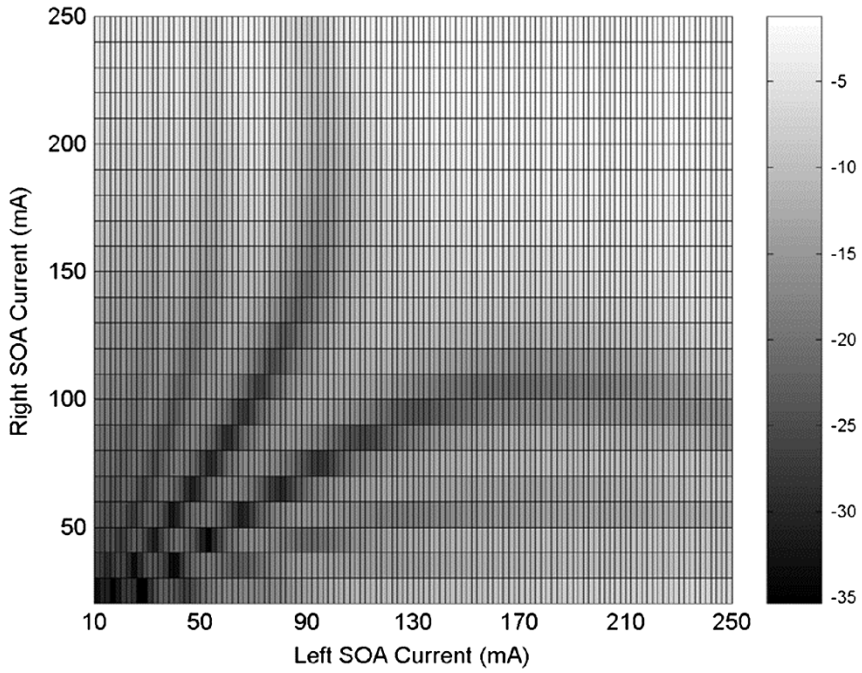

Fig. 8. Extinction map for electrical control of the TAO-WC.

10 dB at 250 mA on either of the SOAs. This can be explained by noting that the large difference in power levels emitted from the two branches of the interferometer when added, even with totally opposite phase, still yields significant power coming out of the interferometer. Hence the performance of the device could be improved by running the SOAs in the interferometer in deeper saturation, i.e., by increasing the optical power of the incoming light, while maintaining the same amount of phase change.

Fig. 9 shows the static electrical transfer functions of the interferometer as a function of integrated laser wavelength. Again, no input signal was present for these measurements. The bias current to the common SOA was kept constant at 200 mA while the bias current to the other SOA in the MZI was varied. As can be seen, the extinction peaks around the material gain peak wavelength (which is approximately 1555 nm).

Typical optical transfer curves for both inverting and noninverting modes of operation, for different input wavelengths, are shown in Fig. 10. In these measurements, the bias of the input preamplifier was kept constant at 80 mA. The interferometer set points were chosen based on the static optical characteristics in Fig. 9, at the minimum for noninverting operation (determined by the bias current of 80 mA), and at the maximum on the left size of the main electrical characteristic notch for inverting mode of operation (55 mA, Fig. 9). Then, the power of the input signal was varied and the output power of the device recorded. Static extinction ratios measured are better than 8 dB in the noninverting and better than 16 dB in the inverting mode of operation. As the transfer curves are highly nonlinear, it is possible to achieve input signal extinction ratio enhancement, as long as the extinction ratio of the input signal is lower that the maximum attainable extinction ratio of the wavelength converter.

The difference in extinction ratios measured for the inverting and noninverting modes of operation can be explained by analyzing the device principle of operation. Due to the cross-gain

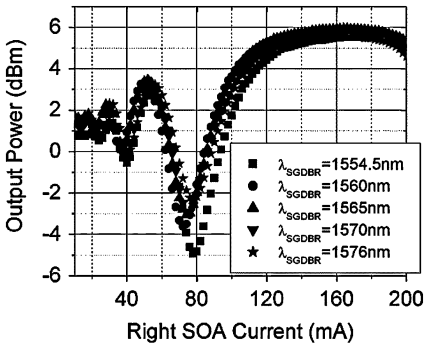

Fig. 9. Static electrical transfer function as a function of wavelength (TAO-WC).

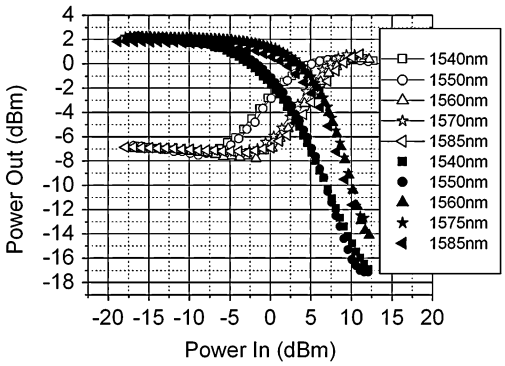

Fig. 10. Optical transfer functions for inverting and noninverting modes of operation (TAO-WC).

effects in the common SOA of the Mach-Zehnder (Fig. 11), the device always yields a higher output extinction ratio in the inverting mode of operation.

For the inverting mode of operation, the output of the MZI is on the high level with no probe signal present (Fig. 12). To reduce the carrier lifetime as much as possible, the bias current of the common SOA should be the higher of the two MZI-SOA bias currents. This bias scheme will result in higher CW signal power at the output of the common SOA. Once the probe signal enters the common SOA, the gain compression will reduce the power of the pump signal in the common MZI branch. This causes two effects—the phase change for the CW signal and the power level equalization between the two branches of the MZI, which therefore allow for better extinction, due to better cancellation of the fields of similar power coming from the two branches of the SOA. In conclusion, in the inverting mode of operation, the two signals are added together when they both carry more power and subtracted when they have similar power levels therefore yielding high extinction ratio. This is illustrated in Fig. 12.

For the noninverting mode of operation, the output of the MZI is on the low level with no probe signal present. To turn the interferometer off, the two SOAs in the MZI have to be biased differently, to yield a relative π phase shift. However, these different bias levels will limit the output extinction at the low level, due to significantly different field intensities in the two interferometer branches (Fig. 11). Once the probe signal enters the common SOA, it will cause the gain compression effect which will reduce the power of the pump signal in the common SOA and the

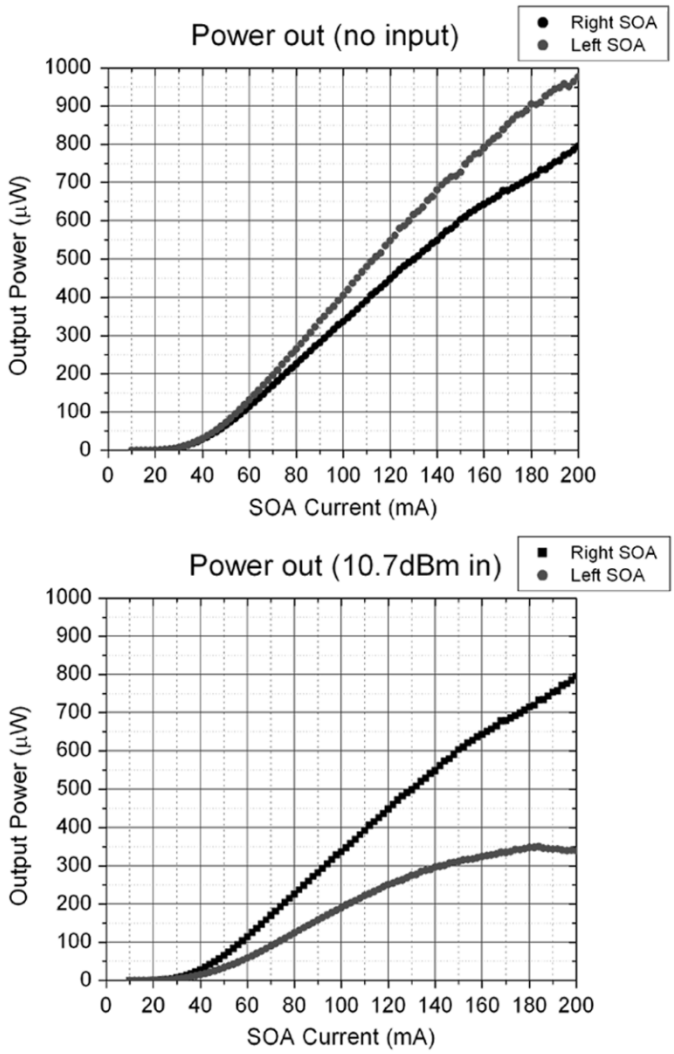

Fig. 11. Gain compression in the common SOA (top) no external signal (bottom) with external signal (TAO-WC).

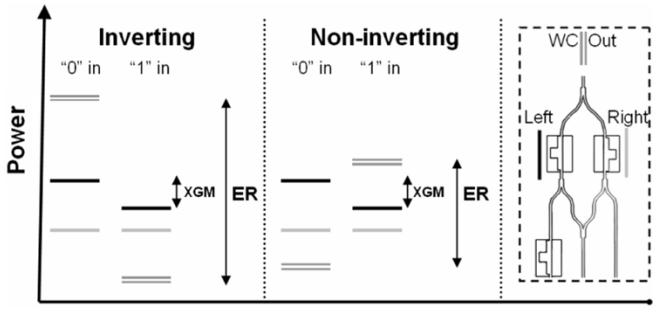

Fig. 12. Extinction ratio analysis for inverting and noninverting modes of operation.

phase change. Consequently, signals from two MZI branches will be added together when power of one of them is reduced by the cross-gain effects of the probe signal. Accordingly, in the noninverting mode of operation, the two signals are being added when they both carry lower optical power, and subtracted when their power levels are different, due to the necessary difference in SOA bias currents to achieve the interferometer OFF state. This effect reduces the maximum obtainable extinction in the noninverting case (Fig. 12).

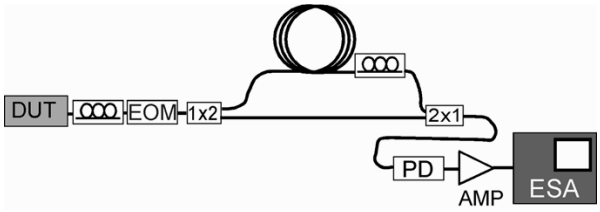

Fig. 13. Linewidth measurement setup.

We can conclude this analysis of the static performance of the wavelength converter by noting that the extinction of the MZI can be improved with the capability of adjusting the phase and the power in the MZI branches independently, as has been done in [20]. That capability would also reduce the differences in output extinction ratios between inverting and noninverting modes of operation.

This extinction ratio analysis holds for the dynamic operation of the wavelength converter as well.

V. Dynamic Performance

As pointed out previously, the key issue for PICs that incorporate integrated lasers is the suppression of coherent back reflections. Even low levels of back reflections can cause significant changes in the laser linewidth, which can degrade the device performance in transmission.

In the first part of this section, TAO-WC linewidth measurement results are presented. Then, results of bit-error rate measurements, the input signal dynamic range, wavelength sensitivity of the wavelength conversion process, bias sensitivity of the wavelength conversion process, dynamic extinction ratio and signal regeneration are discussed.

A. Linewidth

Measuring the linewidth of the device provides useful information about the limitations of the device performance in real networks. Relative intensity noise measured after transmission through fiber indicates that high-frequency white noise determines the transmission properties of a device [21]. In this paper, we determine the linewidth of the TAO-WC device directly by measuring the autocorrelation function of the output light beam. Direct comparison of our results with the linewidth of a commercial widely tunable SGDBR laser enable us to assess the wavelength converter properties as well as investigate the potential back reflection issues with the chip. Although optical low-coherence reflectometry can be used as a more accurate tool to investigate the origins of particular back reflections on chip, the information on the linewidth represents a good way of verifying whether any detrimental reflections are present in the device at all.

The linewidth of a light source can be determined by measuring the autocorrelation function of the output light beam [23]. If the electric field from the output of the device is mixed with the version of the same field that is delayed by some time t, as long as the phases of two fields are well correlated, the fields will add coherently [23].

The schematic of the experimental setup used to measure the linewidth is shown in Fig. 13. The gain section of the tunable wavelength converter's laser is biased at 90 mA, the booster—SOAs are biased at 45 mA, and the MZI-SOAs are biased at 200 mA. The light from the output is coupled through a lens with a built-in isolator, then modulated with a sinusoidal signal whose frequency is 1 GHz. Then the light is split between the two branches of the interferometer, decorrelated by passing the signal from one branch through a spool of fiber, and finally detected by a photodiode, amplified by an electrical amplifier and led to an electrical spectrum analyzer. The reason for spectrally shifting the signal is to eliminate the influence of the $1/f$ noise. The two recombined incoherent fields generate a difference frequency signal which contains the combined FM field noise from both light sources. Therefore, the full width at half maximum of the spectrum measured represents twice the laser linewidth, due to the properties of the Lorentzian line shape [23].

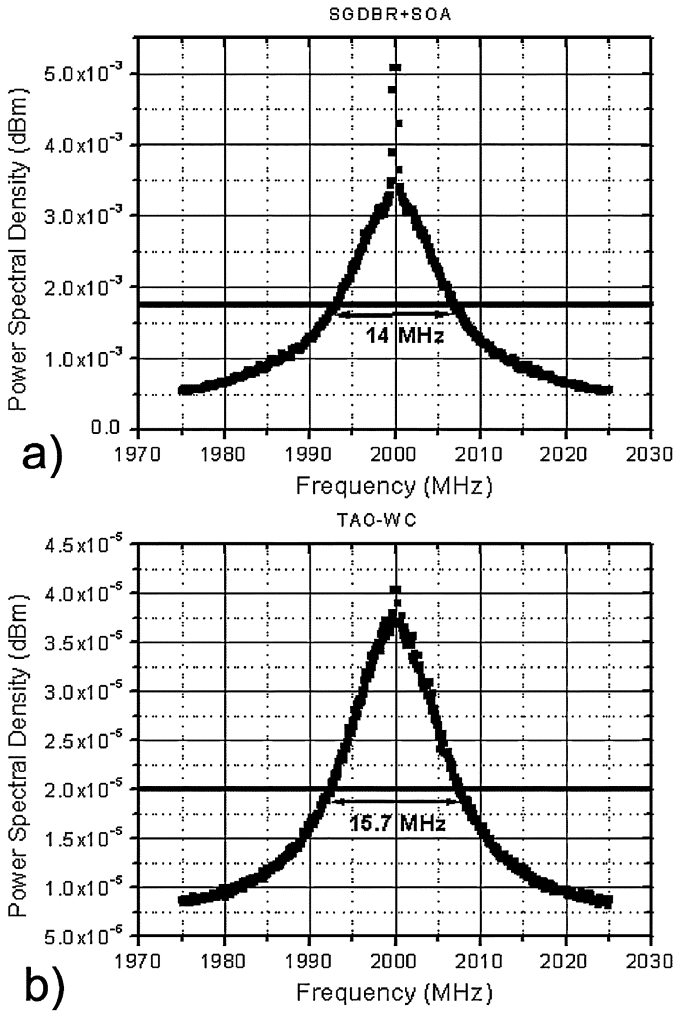

Fig. 14. Linewidth measurement results (a) commercial SGDBR laser. (b) TAO-WC device.

Fig. 14(b) shows the measured FM noise spectrum for the TAO-WC wavelength converter. The linewidth of the device corresponding to this measurement is 7.85 MHz. For comparison, Fig. 14(a) shows the measured FM noise spectrum for an etalon commercial SGDBR laser using the same test setup. The linewidth corresponding to this measurement is 7 MHz. The value measured is consistent with the linewidth values that are

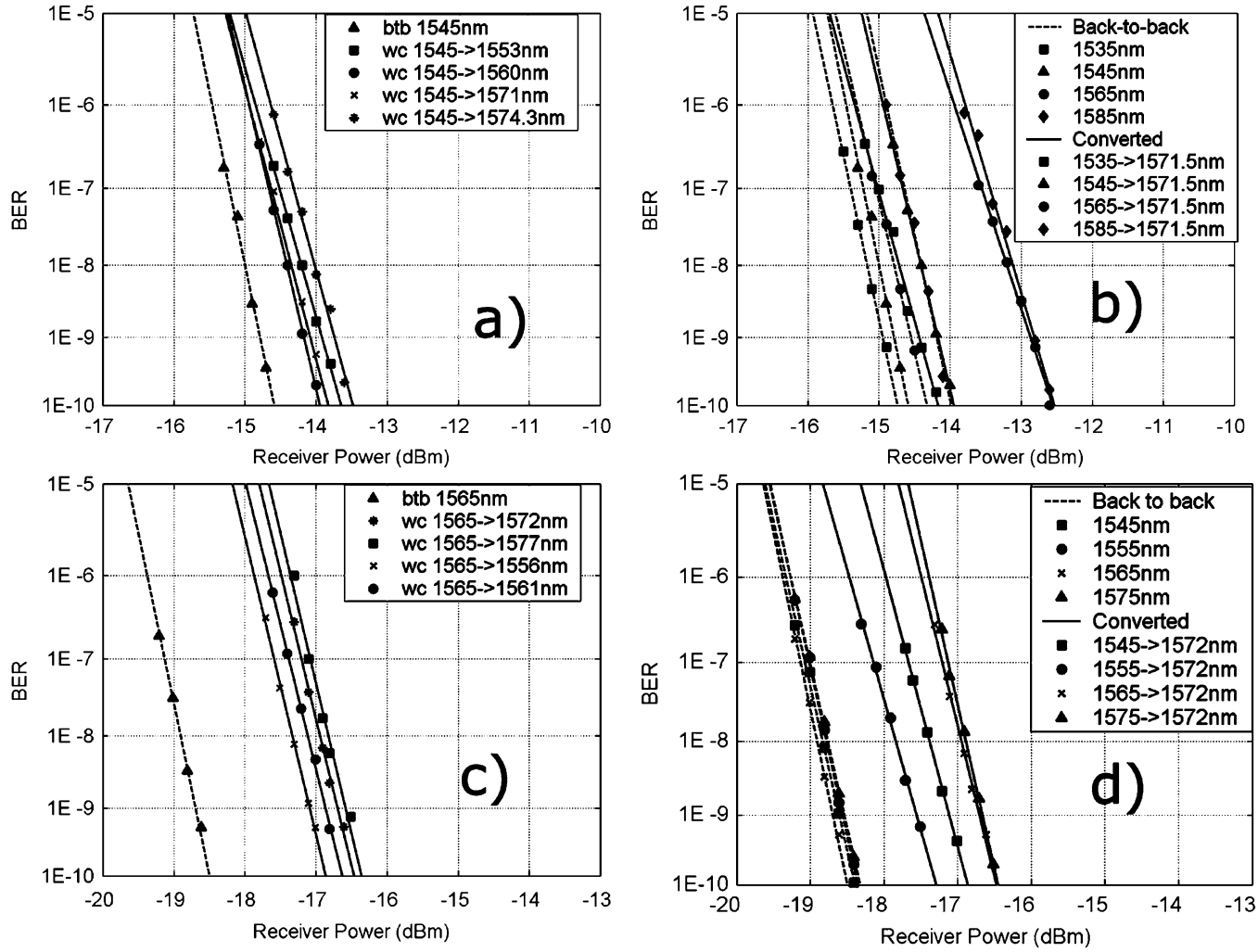

Fig. 15. Results of BER testing for TAOMI and TAO-WC.

specified for this type of laser product. Therefore, the performance of the tunable wavelength converter is free of any influences from coherent back reflections and it is in no way limited by this factor.

B. 2.5 Gbps Wavelength Conversion

The performance of the first generation of the devices (TAOMI-WC) is tested using an Agilent photodiode receiver with a sensitivity of -15 dBm. The input power to the wavelength converter is kept at 4 dBm. The output power of the converter is relatively low (-8 dBm) due to the thermal effects on the MZI-SOA gain, as well as the longer MZI passive sections, when compared to the TAO-WC design. For the first set of measurements, one input wavelength (1545 nm) is chosen, and 2.5 Gbps NRZ $2^{31}-1$ PRBS data are converted onto four different output wavelengths, set by the device (21 nm range). Error-free conversion is obtained with maximum power penalty of 1 dB for the inverting mode of operation, Fig. 15(a). The bias point of the MZI is adjusted for every pair of wavelengths in order to maximize the extinction, thus minimizing the power penalty.

In the subsequent set of measurements, NRZ $2^{31}-1$ PRBS data streams at 2.5 Gbps from different input wavelengths are converted onto one device output wavelength (1571.5 nm). The Mach-Zehnder bias is again optimized for best extinction at each input wavelength. BER curves [Fig. 15(b)] indicate error-free operation over 50 nm input wavelength range, with a maximum power penalty of 1.6 dB. While the upper limit of the input wavelength was set by cross-phase modulation degradation due to finite SOA gain bandwidth, the lower limit was set by the filters available to us (1535 nm). Increase in power penalty and eye noise for input wavelengths above 1565 nm can be attributed, in part, to the input signal-to-noise ratio (SNR) degradation due to our nonoptimum L-band amplifier. Gain in the L band was achieved by using an additional 10 meter long spool of erbium doped fiber in line with our standard C-band EDFA. This noise did not affect our back-to-back measurements, since those were performed without the EDFA. Another cause for power penalty increase in this wavelength range would be higher ASE noise levels as the laser is tuned away from the SOA gain peak.

The second generation of devices (TAO-WC) is tested using a Nortel photodiode receiver with a built-in electrical amplifier, which had a sensitivity of about -18.8 dBm. The output power of the converter is significantly higher in this case (-2 dBm). The main reason for output power increase is the reduced heating of the SOAs in the MZI, due to their larger lat-

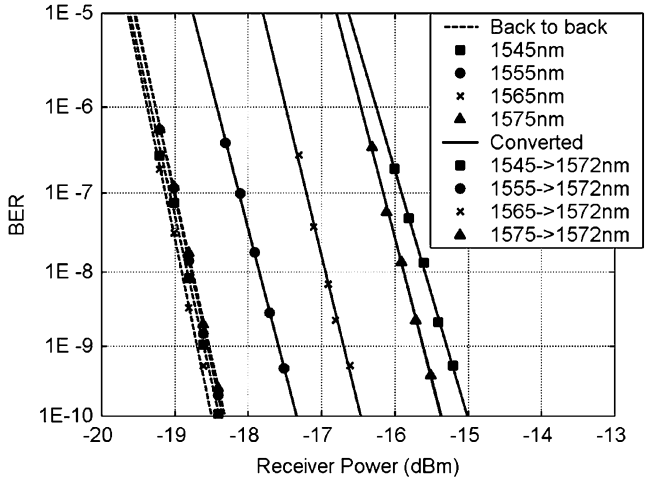

Fig. 16. Wavelength dependence of the BER for TAO-WC.

eral separation (70 μm for TAO-WC, as compared to 17 μm for TAOMI-WC). For the first set of measurements, one input wavelength (1565 nm) is chosen, and 2.5 Gbps data are converted onto 4 different output wavelengths of the device (21 nm range). The bias point of the MZI is adjusted for every pair of wavelengths in order to maximize the extinction, thus minimizing the power penalty. BER curves [Fig. 15(c)] indicate error-free operation with little variation in power penalty as a function of output wavelength. The maximum power penalty was 2 dB. In the subsequent set of measurements, the data streams at 2.5 Gbps from different input wavelengths are converted onto one device output wavelength (1572 nm), again, with optimization of the operating conditions for every wavelength pair. The maximum power penalty again is about 2 dB.

Finally, to investigate the change of power penalty as a function of input wavelength, the TAO-WC is operated with fixed bias currents and input signal powers, and the wavelength of the input signal is varied (Fig. 16). The best power penalty of 1 dB was obtained for the input signal closest to the gain peak of the SOAs at 1555 nm. For this wavelength, the on-chip preamplifier SOA would give the highest possible gain at the input and the effects of gain compression and cross phase modulation in the common SOA of the MZI would be the most pronounced. The power penalty was primarily caused by extinction ratio degradation wavelength dependence, due to finite extinction at the output of <12 dB. The maximum power penalty obtained at far ends of the gain peak was as much as 3 dB, due to further decrease in conversion efficiency and output extinction ratio. Additional power penalty is caused by the pattern dependence of the SOA preamplifiers on chip. The length of the preamplifier SOAs determines the device sensitivity, with longer SOAs decreasing the propagation loss of the input signal. However, long SOAs will always run in saturation, thereby distorting the input signal and introducing the pattern dependence in the converted eye (as seen in Figs. 17 and 18).

C. Device Dynamic Range

Dynamic range of operation can be controlled by the input SOA length and bias, as well as by the bias set point of the MZI. Fig. 17 shows the maximum ER values measured as a function of the data input power. High extinction ratio, greater than 10 dB, can be maintained over 16 dB of input signal power variation. The inset of Fig. 17 also shows the converted eye for -6 dBm input fiber power to a TAO-WC device, corresponding to the converted signal output power of -4 dB in fiber, thereby reamplifying the signal by 2 dB. Different slopes in the eye diagram are due to the different rise and fall times of the pulses, associated with gain recovery time. The input signal wavelength was 1555 nm, and the output signal wavelength was 1565 nm.

The current dynamic range is limited by the passive waveguide propagation losses and available gain of the input SOA. Optimizing the epitaxial heterostructure could yield higher output powers and lower input power requirements, thus increasing the dynamic range and the amount of reamplification. However, care needs to be taken to minimize the pattern dependence effects introduced by the proper design of the preamplifier SOA.

D. Regenerative Properties

Regenerative properties of the SOA-MZI based wavelength converters are based on their highly nonlinear optical transfer characteristics. To quantify the regenerative properties of the tunable wavelength converter (TAO-WC), the input signal's extinction ratio was degraded in a controllable manner by adjusting the EOM bias and the polarization of the light at the input of the electrooptic modulator used to encode the data. This signal, with reduced extinction ratio, was then coupled into the wavelength converter. Significant improvements in the output extinction ratio are obtained—for input ER of 6.33 dB, the converted signal had an extinction of 12.06 dB in the noninverting and 12.33 dB in the inverting mode of operation, Fig. 18. However, decreasing the extinction of the input signal increased the average input power into the common SOA in the MZI and thereby reduced the number of carriers and the gain of the laser signal. Consequently, 6 dBm of input optical power resulted in only -4.4 dBm of the output optical power of the converted signal. On the other hand, device excitation with the high ER signal at the input (12 dB) provided the conversion gain of around 2 dB, with -4 dBm at the optical input and -2 dBm in the converted signal. We believe that this effect could be overcome by increasing the power of the SGDBR laser going into the MZI, thereby constantly keeping the SOAs in the Mach-Zehnder in deep saturation. That would enable the simultaneous signal reamplification and extinction ratio improvement which would qualify the tunable wavelength converter as a 2R regenerator.

E. Chirp Properties

Chirp is the frequency shift occurring in the output pulses of the wavelength converter. This frequency shift appears mainly at the edges of pulses, and is caused by the refractive index modulation in the MZI SOAs. Output chirp is an important parameter for any type of optical regenerator as it will dictate the dispersion-limited transmission distance and/or number of regenerator spans. Low chirp or negative chirp is required for long distance transmission over standard single mode fiber.

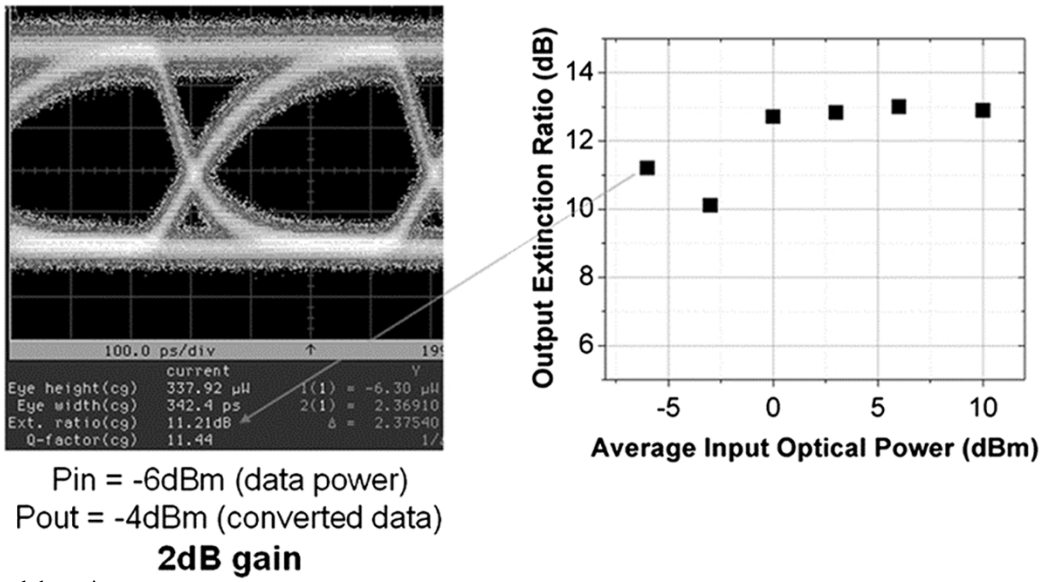

Fig. 17. Input signal dynamic range.

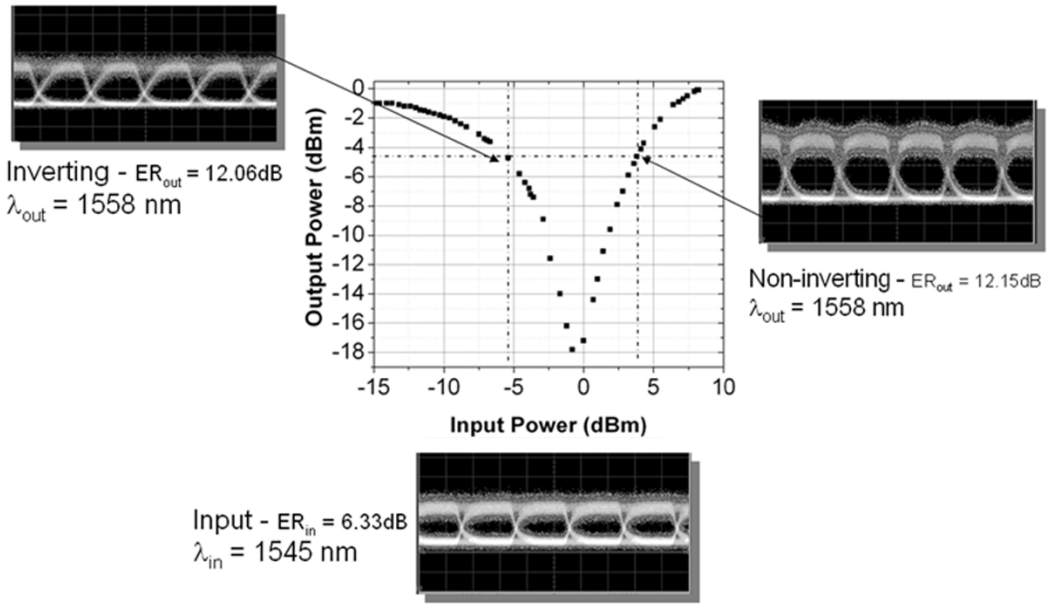

Fig. 18. Example of extinction ratio improvement.

For time-resolved chirp measurements, the TAO-WC MZI's bias currents are optimized for maximum extinction ratio in either inverting or noninverting mode of operation at 2.5 Gb/s. The output of the device is optically filtered and then led into a time-resolved chirp test instrument. The interferometric method used for chirp measurement is based on frequency and amplitude change measurements on two different slopes of the interferometer, in order to obtain the time-resolved frequency change [21]. The optical output from the instrument is connected to a high-speed digital oscilloscope, which is used as part of the setup to perform measurements on the data pattern.

Time-resolved chirp is measured as a function of the input wavelength, output wavelength (set by the integrated on-chip laser) and interferometer bias point (inverting, noninverting and in between). Examples of time-resolved results measured for noninverting (top) and inverting (bottom) mode of operation are shown in Fig. 19. Little input–output wavelength dependence of chirp parameter values is observed across the entire data set. Chirp parameter value and sign depend on the slope of the transfer function of the wavelength converter in the selected regime of operation. For noninverting operation, the average chirp parameter is measured to be -2 for 40 nm input and 22 nm output wavelength range. For inverting mode of operation, the average chirp parameter is measured to be 1–3 for the same output wavelength range. Thus, the performance of the wavelength converter in transmission should consistently reduce the dispersion power penalty if operated in the suitable mode of operation (based on the fiber dispersion parameter). The chirp parameter sign measured is consistent with theoretical predictions [23] and previous results for an XPM-SOA based wavelength converter [25].

F. Dynamic Performance Analysis

Carrier dynamics in the SOAs of the MZI limited the wavelength converter bandwidth to 7 Gbps (for TAO-WC). Dynamic behavior of the chips is a result of the confinement factor of the

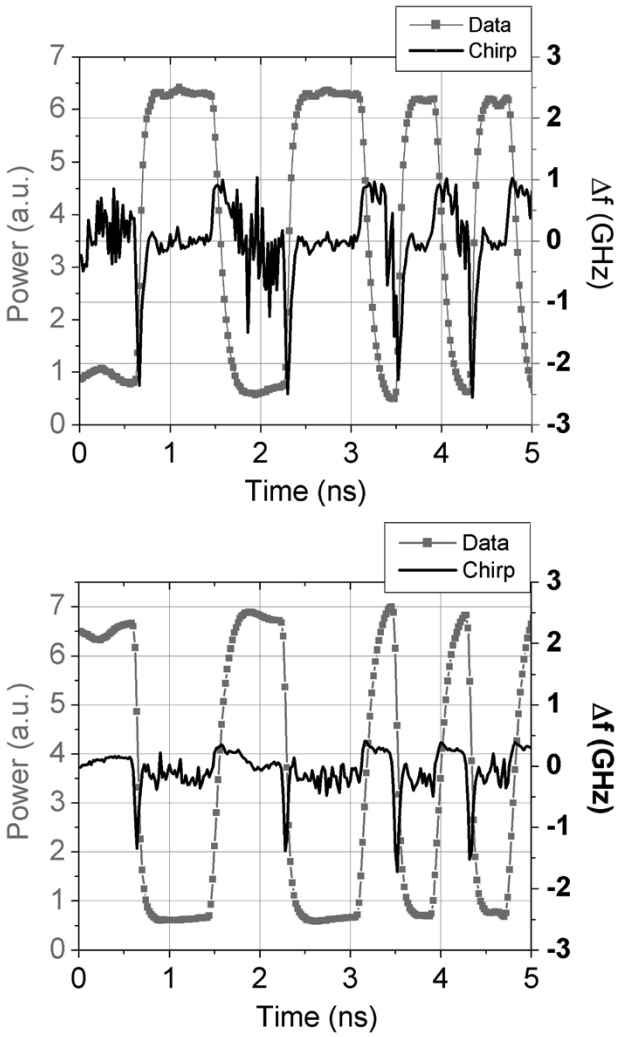

Fig. 19. Examples of time resolved chirp measured: (top) noninverting and (bottom) inverting modes of operation.

SOAs, the gain properties of the quantum wells used, the SOA pump current and the photon density in the SOAs. Increasing the SOA pump currents eventually changes the bandstructure of the quantum wells through thermal effects, which then leads to the reduction in differential gain, thereby increasing the gain recovery time. Therefore, there is an optimum bias current setpoint for the MZI-SOA operation.

The operating speeds observed for TAO-WC device type are higher than those for TAOMI-WC device due to several differences in the device design. First, the length of the passive sections preceeding the MZI-SOA in the TAO-WC design is shorter than that in the TAOMI-WC design, allowing for higher SGDBR-generated CW light intensities to reach the MZI. This high photon density helps to reduce the gain recovery time by increasing the optical pumping of the SOAs in the MZI. The higher speeds are observed in part due to the wider separation of the MZI SOAs in the TAO-WC device, which leads to lower heating of these SOAs, causing the differential gain to remain high.

The main mechanism that can be used to enhance the bandwidth of operation in the offset quantum-well platform is further increase of the photon density in the MZI-SOAs. This has been demonstrated with an improved device design and operation at 10 Gbps in our more recent work [26].

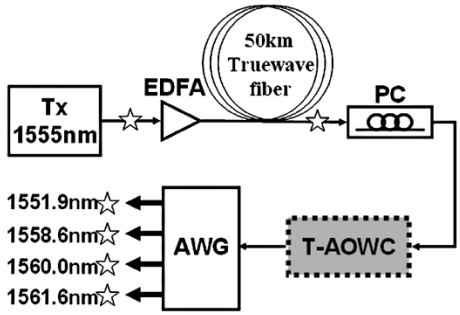

Fig. 20. Schematic of the wavelength routing experiment.

VI. Wavelength Routing Demonstration

As discussed in the introduction, one of the main applications of tunable wavelength converters is for the implementation of optical wavelength routing. Hence, a tunable wavelength converter must be able to reliably convert received signals between different channels in a WDM network, such as the channels determined by the ports of an arrayed waveguide grating router (AWGR). As part of this work, a demonstration of wavelength routing using the TAO-WC device is shown through four different ports in an AWGR, as indicated in the experimental setup schematic, Fig. 20.

A. Experiment

The transmitter consists of a tunable laser operating at 1555 nm, a polarization controller, and a lithium niobate electro-optic modulator. An EDFA is placed after the transmitter to amplify the signal for transmission through 50 km of dispersion shifted Truewave fiber.

Two conical-tipped lensed-fibers on piezo-controlled translational stages are used to couple light into and out of the device. Four wavelengths (1551.9, 1558.6, 1560.0, 1561.6 nm), each corresponding to a different port on the AWGR, are chosen for their placement in the C-band and for their relation to the input wavelength of 1555 nm. Tuning of the device's output wavelength is achieved by current injection through the front, phase, and back mirror sections of the integrated SGDBR laser.

B. Results

For the experimental demonstration, the $2^{31}-1$ PRBS data at 2.5 Gbps is generated using a BERT pattern generator. The optical power measured in the fiber at the input to the device is -2.5 dBm. For each output wavelength, the currents injected through the SOAs of the device's MZI arms are adjusted to maximize the extinction ratio of the wavelength converted signal. The extinction ratio is calculated using the eye diagram obtained by a digital sampling oscilloscope.

Extinction ratios of 12 dB or greater are measured for each of the wavelength converted signals. BER measurements are taken after the transmitter, after the 50 km spool of fiber, and at the output ports of the AWGR for each wavelength using an optically preamplified receiver whose sensitivity was -34.5 dBm. Results of the BER measurements are shown in Fig. 21. Less

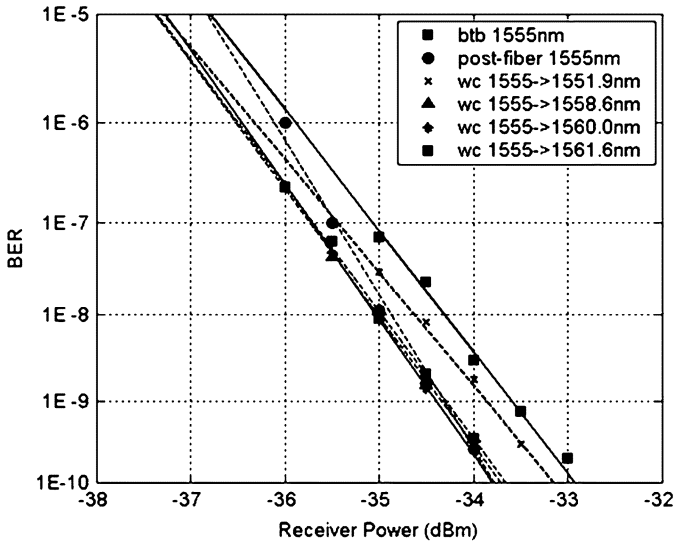

Fig. 21. BER results for the wavelength routing experiment.

than 1 dB of power penalty is observed at a bit-error rate of 10^{-9} for each of the wavelength converted signals.

VII. Conclusion

Monolithically integrated widely tunable wavelength converters are PICs whose function is essential for WDM systems, particularly in applications like optical switching, wavelength routing, and add/drop multiplexing.

In this paper, we discussed the design, fabrication, and characterization of the first fully functional monolithically integrated widely tunable all-optical wavelength converters, based on the SGDBR laser monolithically integrated with MZI-SOA wavelength converters. Error-free wavelength conversion at 2.5 Gbps is demonstrated over 50 nm input and 22 nm output wavelength range, with extinction ratio enhancement and signal reamplification. The devices show linewidth comparable to that of commercial SGDBR lasers, as well as low negative chirp.

By further optimizing the device design, it is possible to additionally improve the device performance, including the maximum data rate, the output wavelength tuning range and input and output powers, while keeping the same simple and robust integration platform and the single-regrowth fabrication process. This has been demonstrated with an improved device design operating over a 35 nm output wavelength range and at 10 Gbps in our more recent work [26].

Acknowledgment

The authors acknowledge Agility Communications for providing growth/AR coating services.

References

[1] X. Pan, J. M. Wiesenfeld, J. S. Perino, T. L. Koch, G. Raybon, U. Koren, M. Chien, M. Young, B. I. Miller, and C. A. Burrus, "Dynamic operation of a three-port, integrated Mach-Zehnder wavelength converter," *IEEE Photon. Technol. Lett.*, vol. 7, pp. 995–997, 1995.

[2] W. Idler, K. Daub, G. Laube, M. Schilling, P. Wiedemann, K. Dutting, M. Klenk, E. Lach, and K. Wunstel, "10 Gb/s wavelength conversion with integrated multiquantum-well 3-port Mach-Zehnder interferometer," *IEEE Photon. Technol. Lett.*, vol. 8, pp. 1163–1165, 1996.

[3] C. Janz, F. Poingt, F. Pommereau, W. Grieshaber, F. Gaborit, D. Leclerc, I. Guillemot, and M. Renaud, "New all active dual order mode (DOMO) Mach-Zehnder wavelength converter for 10 Gbit/s operation," in *ECOC 99*, Nice, France.

[4] L. Spiekman, U. Koren, M. Chien, B. Miller, J. Wiesenfeld, and J. Perino, "All-optical Mach-Zehnder wavelength converter with monolithically integrated DFB probe source," *IEEE Photon. Technol. Lett.*, vol. 9, pp. 1349–1351, 1997.

[5] R. Broeke and M. Smit, "A wavelength converter with integrated tunable laser," in *IPR 2003*, Washington, DC, 2003.

[6] V. Jayaraman, Z. Chuang, and L. Coldren, "Theory, design, and performance of extended tuning range semiconductor lasers with sampled gratings," *IEEE J. Quantum Electron.*, vol. 29, pp. 1824–1834, 1993.

[7] M. Mašanović, V. Lal, J. Barton, E. Skogen, L. Coldren, and D. Blumenthal, "Monolithically integrated Mach-Zehnder interferometer wavelength converter and widely-tunable laser in InP," *IEEE Photon. Technol. Lett.*, vol. 15, pp. 1117–1119, 2003.

[8] M. Mašanović, V. Lal, J. Barton, L. Coldren, and D. Blumenthal, "Wavelength conversion over a 50 nm input and 21 nm output wavelength range using a monolithically integrated tunable all-optical MMI-MZI (TAOMI) wavelength converter," in *Eur. Conf. Optical Commun., ECOC 2003*, Rimini, Italy, Sep. 2003.

[9] B. Mason, J. S. Barton, G. A. Fish, L. A. Coldren, and S. P. Denbaars, "Design of sampled grating DBR lasers with integrated semiconductor optical amplifiers," *IEEE Photon. Technol. Lett.*, vol. 12, pp. 762–764, 2000.

[10] Y. Akulova, G. Fish, K. Ping-Chiek, C. Schow, P. Kozodoy, A. Dahl, S. Nakagawa, M. Larson, M. Mack, T. Strand, C. Coldren, E. Hegblom, S. Penniman, T. Wipiejewski, and L. Coldren, "Widely-tunable electroabsorption-modulated sampled-grating DBR laser transmitter," *IEEE J. Sel. Topics Quantum Electron.*, vol. 8, pp. 1349–1357, 2002.

[11] J. Barton, E. Skogen, M. Mašanović, and L. Coldren, "Widely-tunable high-speed transmitters using integrated SGDBR's and Mach-Zehnder modulators," *IEEE J. Sel. Topics Quantum Electron.*, Sep. 2003.

[12] J. Barton, M. Mašanović, M. Sysak, E. Skogen, J. Hutchinson, D. Blumenthal, and L. Coldren, "A novel, monolithically integrated widely-tunable wavelength converter based on a SGDBR-SOA-MZI transmitter and integrated photodetector," in *Photonics in Switching 2003*, Versailles, France.

[13] J. Hutchinson, J. Henness, L. Johansson, J. Barton, M. Mašanović, and L. Coldren, "2.5 Gb/sec wavelength conversion using monolithically-integrated photodetector and directly modulated widely-tunable SGDBR laser," in *LEOS Annual Meet. 2003*, Tucson, AZ.

[14] C. Joergensen, S. Danielsen, K. Stubkjaer, M. Schilling, K. Daub, P. Doussiere, F. Pommerau, P. Hansen, H. Poulsen, A. Kloch, M. Vaa, B. Mikkelsen, E. Lach, G. Laube, W. Idler, and K. Wunstel, "All-optical wavelength conversion at bit rates above 10 Gb/s using semiconductor optical amplifiers," *IEEE J. Sel. Topics Quantum Electron.*, pp. 1168–1180, 1997.

[15] L. Soldano and E. Pennings, "Optical multi-mode interference devices based on self-imaging: Principles and applications," *J. Lightw. Technol.*, vol. 13, pp. 615–627, 1995.

[16] D. Marcuse, "Reflection loss of laser mode from tilted end mirror," *J. Lightw. Technol.*, vol. 7, pp. 336–339, 1989.

[17] B. Jaskorzynska, J. Nilsson, and L. Thylen, "Modal reflectivity of uptapered, tilted-facet, and antireflection-coated diode-laser amplifiers," *J. Opt. Soc. Amer. B-Opt. Phys.*, vol. 8, pp. 484–493, 1991.

[18] E. Pennings, R. van Roijen, M. van Stralen, P. de Waard, R. Koumans, and B. Verbeck, "Reflection properties of multimode interference devices," *IEEE Photon. Technol. Lett.*, vol. 6, pp. 715–718, 1994.

[19] Y. Gottesman, E. Rao, and B. Dagens, "A novel design proposal to minimize reflections in deep-ridge multimode interference couplers," *IEEE Photon. Technol. Lett.*, vol. 12, no. 12, pp. 1662–1664, Dec. 2000.

[20] E. Gini, E. Gamper, W. Vogt, and H. Melchior, "Monolithic integration of passive waveguides with active SOA's and phase shifters for $\mathrm{lambda} = 1.55\ \mu$m using four step LP-MOVPE growth," in *Proc. 25th Europ. Conf. Opt. Commun. ECOC'99 Conf. Soc. Electr. Electron*, vol. 1, Paris, France, 1999, pp. 174–5.

[21] S. Nakagawa, G. Fish, G. A. Dahl, P. Koh, C. Schow, M. Mack, L. Wang, and R. Yu, "Phase noise of widely-tunable SG-DBR laser," in *Optical Fiber Communications Conf. (OFC). (Trends in Optics and Photonics Series Vol. 86) Tech. Dig. (IEEE Cat. 03CH37403). Opt. Soc. Amer.*, vol. 2, Wash., DC, 2003, pp. 461–2.

[22] R. Saunders, J. King, and I. Hardcastle, "Wideband chirp measurement technique for high bit rate sources," *Inst. Elect. Eng. Electron. Lett.*, vol. 30, pp. 1336–1338, 1994.

[23] L. A. Coldren and S. W. Corzine, *Diode Lasers and Photonic Integrated Circuits*. New York: Wiley-Interscience, 1995.

[24] T. Durhuus, B. Mikkelsen, C. Joergensen, S. L. Danielsen, and K. Stubkjaer, "All-optical wavelength conversion by semiconductor optical amplifiers," *J. Lightw. Technol.*, vol. 14, pp. 942–954, 1996.

[25] S. Cao and J. Cartledge, "Characterization of the chirp and intensity modulation properties of an SOA-MZI wavelength converter," *J. Lightw. Technol.*, vol. 20, pp. 689–695, 2002.

[26] M. L. Mašanović, V. Lal, J. A. Summers, J. S. Barton, E. J. Skogen, L. A. Coldren, and D. J. Blumenthal, "Design and performance of a monolithically-integrated widely-tunable all-optical wavelength converter with independent phase control," *IEEE Photon. Technol. Lett.*, vol. 12, Oct. 2004.

Milan L. Mašanović (S'98–M'04) graduated as a valedictorian from the School of Electrical Engineering, University of Belgrade, Yugoslavia, in 1998. He received the M.S. degree in 2000 and the Ph.D. degree in electrical engineering from the University of California, Santa Barbara, in 2004.

He is currently a Research Scientist at the University of California at Santa Barbara. He authored or coauthored more than 50 papers in the field. His research interests are in the area of InP photonic integration with emphasis on integrated tunable wavelength converters and optical wavelength routing for novel all-optical networks.

Dr. Mašanović received the 2004 IEEE Lasers & Electro-Optics Society (LEOS) Graduate Student Fellowship award as well as the 2003 Best Student Paper Award at Indium Phosphide and Related Materials Conference.

Vikrant Lal (S'00) received the B.S. degree in electrical engineering in August 1999 from the Indian Institute of Technology, Delhi, and the Master's degree in communications engineering from the Electrical and Computer Engineering Department from the University of Maryland, College Park, in August 2001.

He is currently a Ph.D. student in electrical and computer engineering at the University of California, Santa Barbara, working under Prof. D. Blumenthal. His research interests include optical networking, photonic integrated circuits, and all-optical switching.

Joseph A. Summers (S'00) received the B.S. degree in electrical engineering from Northwestern University, Chicago, IL, in 2000 (minor in economics).

He is currently working toward the Ph.D. degree in electrical and computer engineering at the University of California, Santa Barbara. His interests include high-density photonic integrated circuits, and academic outreach.

Jonathon S. Barton (S'00) was born in Sacramento, CA, in 1975. He received the B.S. degree in electrical engineering and material science in 1998 from the University of California, Davis, and the Ph.D. degree in material science from the University of California, Santa Barbara, in 2004.

He is currently a Research Scientist at the University of California at Santa Barbara. His research interests focus on photonic integrated circuits—integrating tunable lasers with semiconductor optical amplifiers and modulators.

Erik J. Skogen was born in Minneapolis, MN, in 1975. He received the B.S. degree from Iowa State University in 1997, and the M.S. and Ph.D. degrees from the University of California, Santa Barbara, in 1999 and 2003, respectively.

After working as a Research Scientist at the University of California, Santa Barbara, he joined Sandia National Laboratories, Albuquerque, NM, in January 2005. His research interests include widely tunable semiconductor lasers, monolithic integration for photonic integrated circuits, crystal growth by MOCVD, and quantum-well intermixing.

Lavanya G. Rau received the Ph.D. degree from the University of California, Santa Barbara (UCSB), in 2003. Her dissertation focused on ultrafast wavelength conversion using cross-phase modulation in nonlinear fiber and its application in future high-speed photonic networks.

She is currently a Postdoctoral Researcher with the California Institute for Telecommunications and Information Technology, University of California at Irvine. Her present work involves evaluating the regenerative nature of all-optical 3R regenerators in the presence of jitter and noise.

Larry A. Coldren (S'67–M'72–SM'77–F'82) received the Ph.D. degree in electrical engineering from Stanford University, CA, in 1972.

After 13 years in the research area at Bell Laboratories, he was appointed Professor of Electrical and Computer Engineering at the University of California at Santa Barbara (UCSB) in 1984. In 1986, he assumed a joint appointment with Materials and Electrical and Computer Engineering and, in 2000, the Fred Kavli Chair in Optoelectronics and Sensors. He is also Chairman and Chief Technology Officer of Agility Communications, Inc. At UCSB, his efforts have included work on novel guided-wave and vertical-cavity modulators and lasers, as well as the underlying materials growth and fabrication technology. He is now investigating the integration of various optoelectronic devices, including optical amplifiers and modulators, tunable lasers, wavelength converters, and surface-emitting lasers. He has authored or coauthored more than 500 papers, five book chapters, and one textbook, and has been issued 32 patents.

Dr. Coldren is a Fellow of the Optical Society of America (OSA) and a Member of the National Academy of Engineering.

Daniel J. Blumenthal (M'97–F'03) received the B.S.E.E. degree from the University of Rochester, New York, in 1981, the M.S.E.E. degree from Columbia University, New York, in 1988, and the Ph.D. degree from the University of Colorado, Boulder, in 1993.

In 1981, he worked at StorageTek, Louisville, CO, and from 1993 to 1997, he was Assistant Professor with the School of Electrical and Computer Engineering, Georgia Institute of Technology, Atlanta. He is currently a Professor with the Department of Electrical and Computer Engineering, University of California at Santa Barbara. He is the Principle Investigator for the Defense Advanced Research Projects Agency (DARPA) Department of Defense (DoD)-N LASOR project and currently serves on the Board of Directors for National LambdaRail (NLR), a national footprint optical network research infrastructure. His research areas are optical communications, photonic packet-switched and all-optical networks, all-optical wavelength conversion, optical subcarrier multiplexing, integrated optic chip-scale wavelength-division multiplexing (WDM), and nanophotonic technologies. He has authored or coauthored more than 160 papers in these and related areas, as well as coauthored the book *Tunable Laser Diodes and Related Optical Sources*.

Dr. Blumenthal is a Member of the Optical Society of America (OSA). He is the recipient of a 1999 Presidential Early Career Award for Scientists and Engineers (PECASE) from the White House and the DoD, a 1994 NSF Young Investigator (NYI) Award, and a 1997 Office of Naval Research Young Investigator Program (YIP) Award. He is an Associate Editor for the IEEE PHOTONICS TECHNOLOGY LETTERS and has served as Associate Editor for the IEEE TRANSACTIONS ON COMMUNICATIONS. He was a Guest Editor for the JOURNAL OF LIGHTWAVE TECHNOLOGY Special Issue on Photonic Packet Switching Systems (December 1998) and Guest Editor for the IEEE JOURNAL OF SELECTED AREAS IN COMMUNICATIONS Special Issue on High-Performance Optical/Electronic Switches/Routers for High-Speed Internet. He also served on numerous other technical program committees, including the Conference on Optical Fiber Communications (OFC) from 1997 to 2000 and the Conference on Lasers and Electro-Optics (CLEO) from 1999 to 2000.